Search for anomalous neutral current coherent-like single-photon production in MicroBooNE

The MicroBooNE Collaboration*

June 13, 2024

Abstract

This note describes progress towards the first experimental search for neutrino-induced neutral current coherent single-photon production (NC coherent 1γ). The search makes use of data from the MicroBooNE's 85-tonne active mass liquid argon time projection chamber detector, situated in Fermilab's Booster Neutrino Beam, with an average neutrino energy of $\langle E_\nu \rangle \sim 0.8$ GeV. A selection targeted on candidate neutrino interactions with a single photon-like electromagnetic shower in the final state and no visible vertex activity was developed to search for this rare NC coherent 1γ process.

1 Introduction

Neutrino-induced NC coherent single-photon production is predicted to be a sub-dominant source of single photons in neutrino-argon scattering below 1 GeV [1]; the dominant single-photon production process in this energy range is that of NC resonance production of Δ baryons followed by Δ radiative decay [2], expected to be roughly an order of magnitude larger than NC coherent single-photon production on argon. Although this NC coherent 1γ process is predicted in the Standard Model (SM), it has never been directly searched for or observed in neutrino scattering.

In this note, we present developments towards the first experimental search for neutrino-induced NC coherent single-photon (NC coherent 1γ) production on argon with an average neutrino energy of $\langle E_\nu \rangle \sim 0.8$ GeV. Much like MicroBooNE's[3] previous search for NC Δ baryon production and radiative decay [4], this measurement serves as another test for photon-like interpretations of the MiniBooNE "low energy excess" [5].

The interaction final state targeted in this analysis is defined as:

$$\nu(\overline{\nu}) + \mathrm{Ar}_{gs} \rightarrow \nu(\overline{\nu}) + \mathrm{Ar}_{gs} + \gamma \tag{1}$$

where Ar_{gs} represents the struck and residual (argon) nucleus, which remains in the ground state after scattering. Due to the coherent (low momentum transfer) nature of the interaction, the outgoing photon tends to have has a forward direction relative to the beam. Thus by searching for a distinct electromagnetic shower topology in the forward direction, the photon is identifiable in the MicroBooNE detector. No other observable sactivity is expected in the final state, and this informs the signal selection requirement strategy.

*Email: microboone_info@fnal.gov

This document was prepared by MicroBooNE Collaboration using the resources of the Fermi National Accelerator Laboratory (Fermilab), a U.S. Department of Energy, Office of Science, Office of High Energy Physics HEP User Facility. Fermilab is managed by Fermi Research Alliance, LLC (FRA), acting under Contract No. DE-AC02-07CH11359.

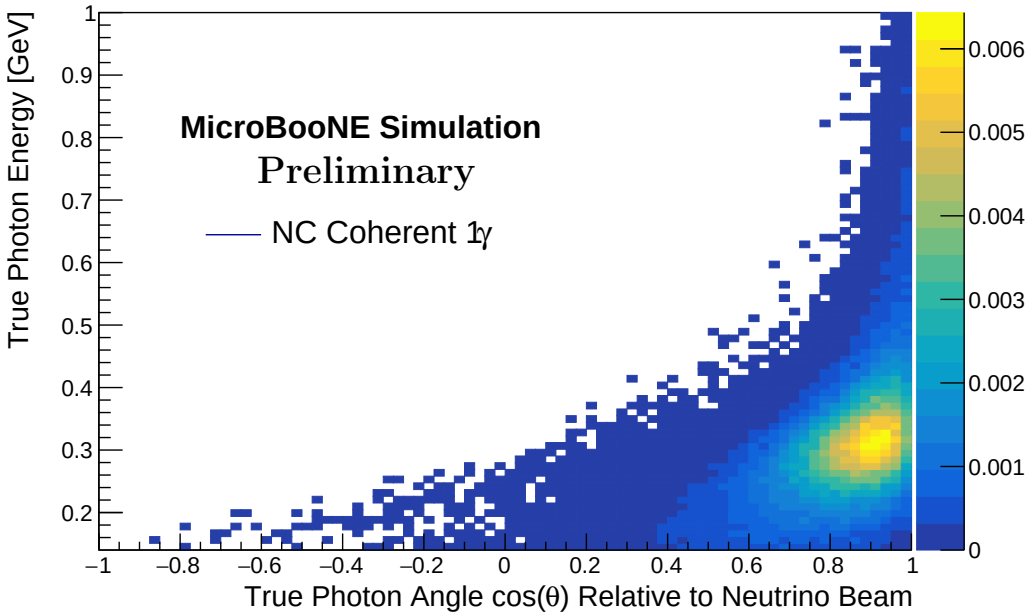

Figure 1: *The area-normalized 2D distribution of the true energy and angle with respect to the beam of outgoing photons in NC coherent* 1γ *events. It highlights the phase space of the outgoing photon, with a forward nature and peak energy at* ~ 0.3 *GeV.*

2 Analysis Overview

The theoretical model of this process was proposed and described in detail in [1], with a predicted total cross-section of $\frac{\sigma}{A} \sim \mathcal{O}(10^{-43}\text{cm}^2)$ where A is the atomic number of the target nucleus. This model is not implemented in the GENIE `v3.0.6` generator incorporated in MicroBooNE software; instead it has been successfully implemented in an updated GENIE version [6][1]. Figure 1 shows the distribution of the simulated outgoing photons as a function of the true photon energy and its angle with respect to the neutrino beam direction, highlighting the forward nature of the outgoing photon from the coherent interaction.

The analysis was designed to be a blind analysis. It was developed using mainly Monte Carlo (MC) simulation overlay samples. A small subset of the data, about 10% of the full Runs 1-3 data, was accessible during the analysis development stage to allow for the iteration of the analysis if necessary. A sideband sample was also defined, and the analysis was fully frozen and validated on the sideband sample using Runs 1-3 data before the signal region was unblinded.

3 Event Selection

Driven by the rarity of the targeted signal, a series of selections, including traditional and gradient-boosted decision-tree (BDT) based selections, were developed with the goal of maximizing background rejection efficiency. The following sections present the detailed selections and tools developed for this analysis.

[1]More specifically the signal simulation used in this analysis is done with a development branch of GENIE with source code at *NCGammaFix* branch of git repository: GENIE generator.

3.1 Topological and Preselection Stages

The event selection starts with a topological selection on outputs from the Pandora reconstruction framework[7], specifically requiring one reconstructed shower and zero reconstructed tracks, proton, muon or pion-like, (demoted $1\gamma 0p$), which is the expected topology for NC coherent 1γ signal in the detector. This topological requirement selects 28.1% of simulated NC coherent 1γ events; the remainder of the events do not pass the selection cut because 32.7% of the signal events are reconstructed with no track or shower by Pandora, while 39.2% are reconstructed with either ≥ 1 tracks or ≥ 2 showers. Then, preselection cuts are applied in order to remove obvious backgrounds. The preselection cuts require that the reconstructed shower energy be larger than 50 MeV to remove Michel electrons from cosmic muon decays. Additionally a fiducial volume cut of at least 2 cm away from the space charge boundary [8] is made on the reconstructed shower start, in order to remove showers originating from particles scattering into the TPC. Relative to the topological stage, the preselection cuts further remove 33.9% of the overall background - mostly dirt and cosmic ray background - while preserving 98.6% of the signal. At preselection, 27.7% of the NC coherent 1γ signal remains out of all simulated signal events in the TPC, and the corresponding signal to background ratio is about $1:2696$. Figure 2 shows the predicted NC coherent 1γ signal scaled by a factor of 2500 and the nominal predicted background at preselection, highlighting the rarity of the signal and different regions of phase space in reconstructed shower energy populated by the signal and backgrounds.

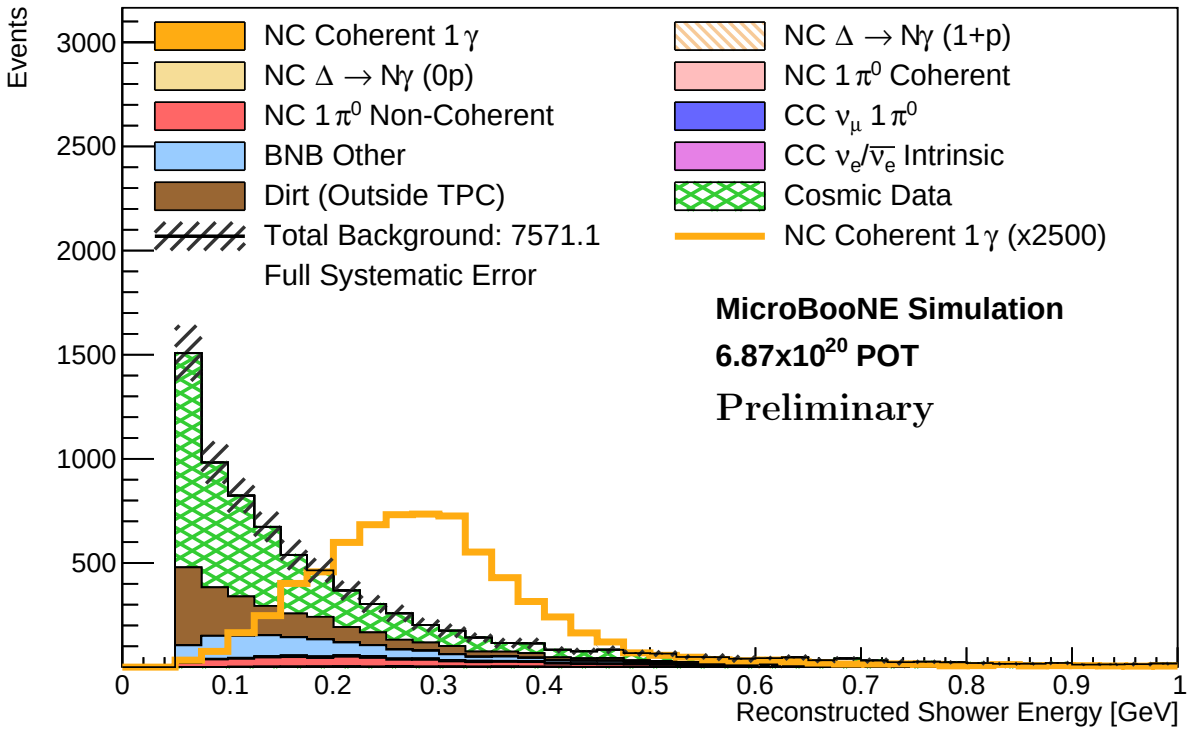

Figure 2: *MC simulation predicted background distribution as a function of the reconstructed shower energy at preselection. The orange histogram overlaid shows the distribution of NC coherent 1γ signal scaled by 2500 times for it to be visible. At this stage, the signal and backgrounds populate different regions of phase space in the reconstructed shower energy.*

3.2 Event-level Boosted Decision Tree Based Selection

At preselection, BDTs are developed and optimized to further differentiate the signal from background events. There are in total six (6) tailored BDTs developed using the XGBoost library [9], each trained with variables derived from reconstructed objects. Every BDT targets a different background and thus is trained with different labeled background events. There are four BDTs trained with event-level variables, which are variables unique to the reconstructed objects in event (such as shower energy, shower start position ..etc..), and two BDTs trained with cluster-level variables associated with clusters of reconstructed 2D hits in each event that were not successfully matched into a 3D shower or track object.

The largest background contributions remaining at preselection are cosmic-ray background, dirt events ($\sim 50\%$ of which are π^0 events), BNB Other, and NC non-coherent $1\pi^0$, ordered by the size of predicted contributions in decreasing order. Three event-level BDTs are employed to target these backgrounds, and another BDT is designed to specifically target the electron background from CC interactions induced by the intrinsic $\nu_e/\overline{\nu}_e$ in the beam. To enhance the ability of BDTs in learning the differences between NC coherent 1γ events and backgrounds, all four BDTs are trained with selections of events passing the preselection requirements. The same NC coherent 1γ overlay sample is used as the "signal" during training in four BDTs. The background definitions used and the key features in training the four BDTs are described below:

Cosmic BDT: The goal of the cosmic BDT is to differentiate NC coherent 1γ signal from misidentified cosmic backgrounds. The cosmic BDT trains on BNB external data as background, and makes use of the fact that cosmic rays usually travel from the top of the detector down to Earth vertically.

CC ν_e BDT: CC ν_e BDT aims to remove reconstructed showers originating from electrons instead of photons, and trains on simulated, preselected CC $\nu_e/\overline{\nu}_e$ events. One key handle for photon/electron separation is the shower dE/dx. Most photons in the energy range relevant to this analysis lose energy through e^+e^- pair production; these then further radiate, producing an electromagnetic shower. Compared to the electron shower, whose dE/dx at the shower start is similar to the dE/dx of a minimum ionizing particle (MIP) around 2 MeV/cm, the photon shower start has $dE/dx \sim 4$ MeV/cm.

CC ν_μ focused BDT: The CC ν_μ focused BDT aims to remove any backgrounds other than the cosmic, NC Δ radiative decay, CC $\nu_e/\overline{\nu}_e$ and NC $1\pi^0$. Among these background events, about 76% are CC $\nu_\mu/\overline{\nu}_\mu$ events, 60% of which are CC events without π^0 exiting the nucleus, and for which the muon is mis-reconstructed as a shower. Since muons are MIPs, variables such as shower dE/dx, averaged energy per hit in the reconstructed shower, and Pandora shower score (a metric of how "shower-like" the object is) are of importance for the separation of mis-identified muons from the true coherent single photons.

NC $1\pi^0$ BDT: NC $1\pi^0$ background is harder to remove compared to cosmic and other ν-induced backgrounds because in most cases the reconstructed shower in mis-identified NC $1\pi^0$ is indeed from a true photon (most likely the leading photon from π^0 decay). There are a variety of reasons that could lead to single shower reconstruction in π^0 sample: 1) The second shower from π^0 decay is not visible in the detector; this could happen when the photon is absorbed by the medium, leaves the detector before pair-producing, or is too low energy to be detected. 2) The second shower deposits energy in the detector but the 3D reconstruction fails; this could happen when the cluster-matching across planes in Pandora fails. 3) The hits from the second photon are reconstructed in 3D but not associated with the neutrino interaction; this happens when cosmic-rays interfere with the energy deposition on one or more planes. To mitigate failure case (2), a

cluster-level second-shower veto (SSV) BDT is developed following the exact same approach as in Ref [4] to identify the possible presence of the second shower that misses reconstruction, and is described in a later section.

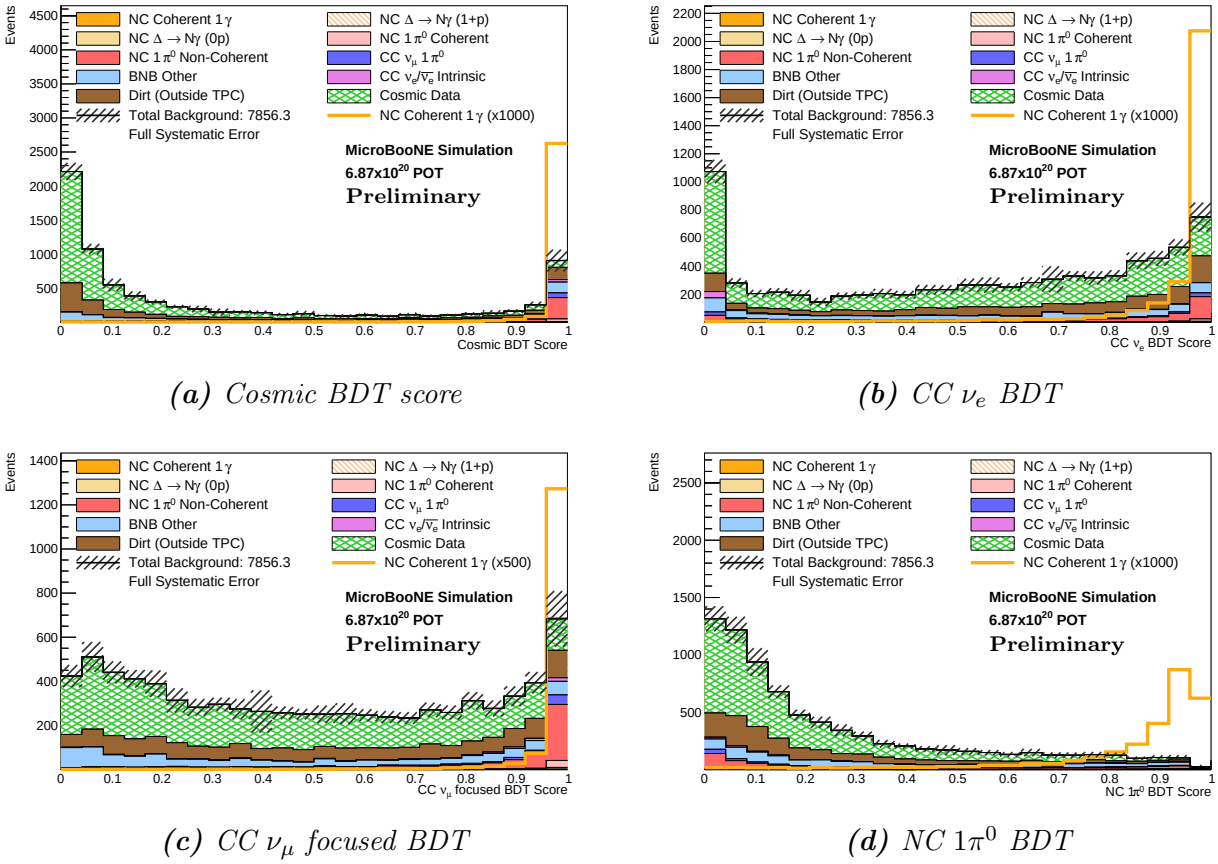

(a) Cosmic BDT score

(b) CC ν_e BDT

(c) CC ν_μ focused BDT

(d) NC $1\pi^0$ BDT

Figure 3: *The BDT classifier scores for (a) the Cosmic BDT; (b) CC ν_e BDT; (c) CC ν_μ focused BDT and (d) NC $1\pi^0$ BDT. Higher scores indicate more NC coherent 1γ signal-like events. The stacked histograms show the predicted background distribution, while the yellow hollow histogram represents the distribution for the NC coherent 1γ signal, both at pre-selection stage. The signal histogram is significantly scaled for visual purposes by 1000 times in (a), (b), (d) and by 500 times in (c).*

The outputs of the event-level BDTs are scores in the range of [0,1]; a higher event-level BDT score indicates the event is more NC coherent 1γ signal like. Figure 3 shows the predicted BDT score distributions at preselecetion stage. The NC coherent 1γ signal is scaled up in order to highlight the separation between the signal and the targeted background in the BDT responses.

Cut positions for these four event-level BDTs are optimized towards maximizing the statistical significance of the NC coherent 1γ signal, i.e. $\frac{N_{\text{sig}}}{\sqrt{N_{\text{bkg}}}}$. The set of cuts chosen to maximize signal selection efficiency was Cosmic BDT ≥ 0.990, CC ν_e BDT ≥ 0.885, CC ν_μ BDT ≥ 0.992 and NC $1\pi^0$ BDT ≥ 0.891. A selection of events pass requirements on these four BDTs if their BDT scores are higher than the corresponding cut values and comprise the "semi-final" selection.

3.3 Cluster-level Boosted Decision Tree Based Selection

Cluster-level BDTs are designed to identify activities of interest that are missed by Pandora pattern recognition. There are two cluster-level BDTs employed in this analysis. First, a second-shower veto (SSV) BDT targets the missing second shower from π^0 decay in π^0 backgrounds.

Second, a proton-stub veto (PSV) BDT aims to identify proton activity near the shower vertex, in order to remove non-coherent backgrounds. Both BDTs build on hits that are not reconstructed in 3D by Pandora: individual scattered hits are clustered by DBSCAN together to form candidate clusters of interest which get classified by the BDTs.

3.3.1 Second shower veto BDT

The SSV BDT targets the second shower from the π^0 decay in the detector, which has an expected topology of a sparse cascade of hits near the primary reconstructed shower. The reconstructed calorimetric and spatial variables associated with second shower candidate clusters are the inputs to the SSV BDT. More specifically, second shower candidate clusters that are truth-matched to a different photon from the primary reconstructed shower in the NC $1\pi^0$ sample serve as the training signal, while second shower candidate clusters formed in simulated NC coherent 1γ events are used as training background. The output of the BDT is a score assigned to each cluster from 0 to 1. The higher the score, the higher the probability that the cluster originates from a photon from π^0 decay. The result of SSV BDT is not directly used in event selection; instead, high-level variables such as the maximum SSV BDT score of all clusters on each plane are input variables to the NC $1\pi^0$ BDT. Figure 4 shows the distribution of the maximum SSV BDT scores of all clusters formed in events.

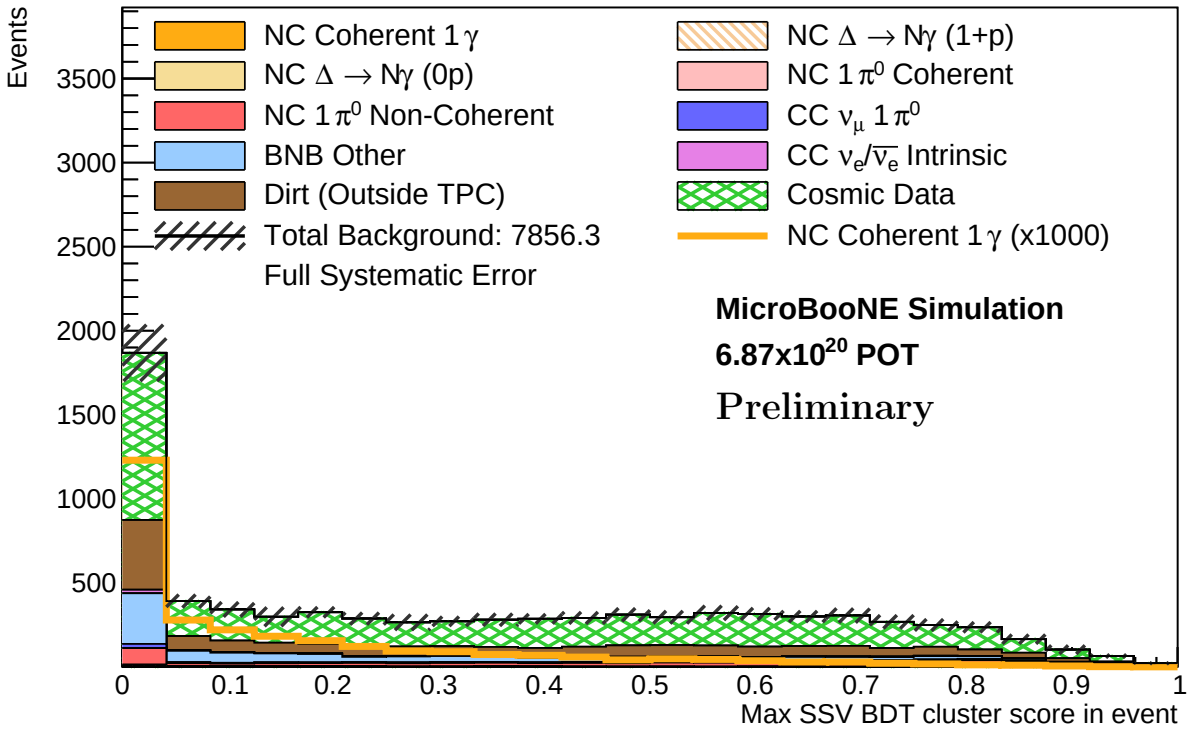

Figure 4: *Distribution of the maximum SSV BDT score of all clusters formed in events at preselection stage. Nominal predictions for backgrounds are stacked in the colored histograms, while the signal prediction is scaled by a factor of 1000 and plotted separately in the yellow hollow histogram. Higher score means a higher probability of a second shower present in the event. Note that, if no second shower candidate cluster is formed in an event, the maximum SSV BDT score for this event is set to zero.*

3.3.2 Proton stub veto BDT

Besides the SSV score, another handle is leveraged to aid in the rejection of background: tiny proton traces. Pandora's proton identification threshold in this analysis is around 40 MeV of kinetic energy; however, hand scanning of NC Δ radiative decay events shows visible true proton-like activity on one or more planes near the reconstructed shower in some $1\gamma 0p$ events. These proton-like activities usually sit very close to the backward projection of the shower direction. The PSV BDT is designed to identify such indications of protons missed by reconstruction, through which we can remove non-coherent backgrounds, specifically misidentified NC backgrounds with protons exiting the nucleus.

The building block of the PSV BDT is proton candidate clusters, similarly to the SSV BDT. Since most protons that are missed by the reconstruction are low energy, and proton tracks are expected to be very straight with dense energy deposition, proton candidate clusters are required to be dense during the DBSCAN clustering. Due to many small low energy cosmic and EM clusters the PSV BDT must be efficient in correctly identifying true proton clusters from substantial amount of background clusters arising from other activity. Two handles help solve this problem: the geometric relation between true proton candidate clusters and the reconstructed shower, and the distinct calorimetric profile of proton track.

The cartoon in Fig. 5 shows a potential geometric relation between a proton candidate cluster and the reconstructed shower on a plane. In backgrounds that have true protons exiting the nucleus and reconstructed shower from a true photon, the proton cluster is expected to intersect the line of backward projection of the reconstructed shower. This means the minimum perpendicular distance from the candidate cluster to the direction of the primary reconstructed shower, i.e. the impact parameter of the cluster, should be small for the proton candidate clusters, given the imperfect reconstructed shower angle resolution. Additionally, the PSV BDT also takes advantage of the straightness and the Bragg peak signature expected for a proton track to identify true proton clusters.

The simulated NC Δ radiative decay sample is used to train the PSV BDT: proton candidate clusters in the NC Δ sample that are truly from protons are used as training signals, while the remaining candidate clusters are the training background. Unlike the SSV BDT, which is not used as a selection cut, a cut is applied directly on the derived PSV BDT output to further improve the signal-to-background ratio after the semi-final selection.

The derived PSV BDT output used is the maximum PSV BDT score of all proton candidate clusters on plane 0 and plane 2 (abbreviated as "maximum PSV score on Planes 02"). Plane 1 was omitted for this analysis as candidate clusters showed poorer agreement with open data, future updates aim to address this. Figure 6 shows the distribution of the maximum PSV score on Planes 02 for the predicted background at preselection stage. As expected, the NC coherent 1γ signal and most of the background pile up on the left, while the right corner is most populated by the NC non-coherent $1\pi^0$. The distribution of the same variable with the cosmic, CC ν_e and CC ν_μ-focused BDT requirements applied is shown in Fig. 7. The resulting sample is a photon-rich sample dominated by the NC non-coherent $1\pi^0$s. The peak near 1 is mostly populated by NC non-coherent $1\pi^0$ background, highlighting the strong separation power of the PSV BDT. The NC coherent 1γ signal and majority of the NC coherent $1\pi^0$ background cluster at low BDT score regions due to their coherent nature, as expected.

The requirement on the maximum PSV score on Planes 02 is applied to events in the semi-final selection, and the cut value is optimized to maximize the signal significance with the neutrino flux and neutrino interaction uncertainties. The optimized cut position for the maximum PSV score on Planes 02 is found to be 0.2. Events that have a maximum PSV score on Planes 02 less than the cut value (0.2) comprise the final signal selection.

Figure 8 shows the rejection efficiency of the PSV BDT on simulated NC non-coherent $1\pi^0$, NC $\Delta \rightarrow N\gamma$ (1+p) and $0p$. The rejection efficiency is evaluated by calculating the fraction of

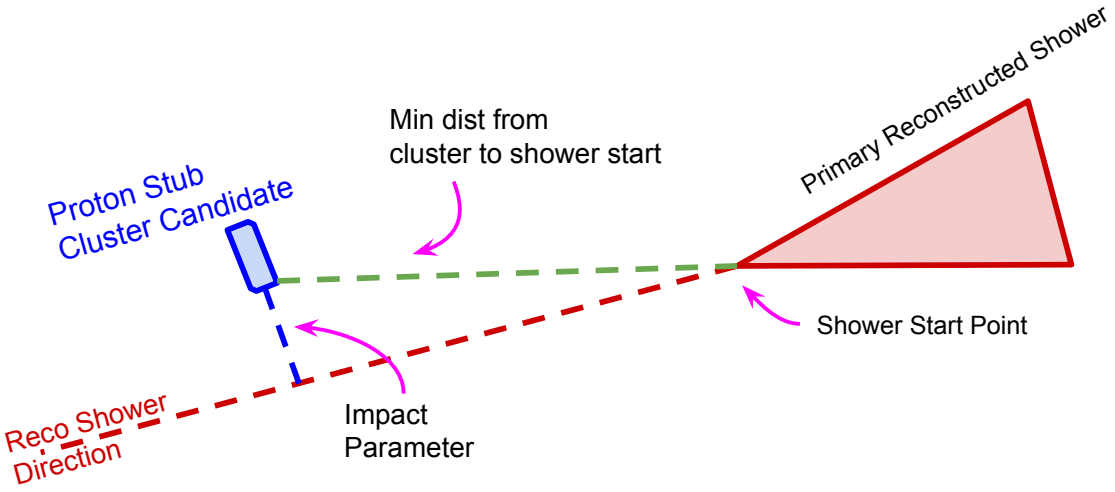

Figure 5: *Cartoon showing the relative position of a proton candidate cluster to the primary reconstructed shower on a plane. Two important variables for the PSV BDT are also highlighted: the minimum distance between the proton cluster and the reconstructed shower start, and the impact parameter of the candidate cluster to the shower direction. If the proton stub candidate is indeed from a proton that comes from the same vertex as the reconstructed shower, the impact parameter is expected to be close to zero, assuming the reconstructed shower direction is accurate.*

events that pass the PSV BDT requirement in each bin, relative to selected events passing the topological, preselection stage, and cosmic, CC ν_e and CC ν_μ BDT requirements. We observe that the PSV yields a high rejection efficiency on protons at low energies on all three samples, with an average of approximately 70% rejection efficiency for protons with kinetic energy less than 50 MeV.

3.4 Final Selections

We first show the prediction at the semi-final stage in three variables that highlight the reconstructed shower energy and angle, as well as the PSV features of signal and backgrounds in Fig. 9. The selection has a reconstructed shower distribution with an energy peak of around 300 MeV and a very forward angle, which is expected for the NC coherent 1γ signals. As expected, the NC non-coherent $1\pi^0$ is the most dominant background, and the PSV distribution suggests that an additional requirement on the PSV variable could further reject a large fraction of it.

Table 1 shows all backgrounds and signal predictions for the semi-final and final selection, normalized to 6.87×10^{20} POT, expected for Runs 1-3. At the semi-final stage, there are a total of 55.8 predicted background and 1.3 signal events, leading to a signal-to-background ratio of 1:42. The PSV requirement further improves the signal-to-background ratio to 1:30 by filtering out almost half of the NC non-coherent $1\pi^0$ background. Figure 10 shows the selection efficiency for the simulated NC coherent 1γ signal in the active TPC at different stages, as a function of the true energy and angle of the outgoing photon.

The selection efficiencies for all background categories at different analysis stages are included in Tab. 2, calculated relative to predictions after the topological selection. The event-level BDTs successfully reject all types of backgrounds by a large fraction, especially the intrinsic CC ν_e, BNB Other, dirt and cosmic backgrounds. Transitioning from semi-final stage to final selection stage, the cut on the PSV BDT acts mostly on the NC $\Delta \to N\gamma$ (1+p), NC $\Delta \to N\gamma$ (0p) and NC

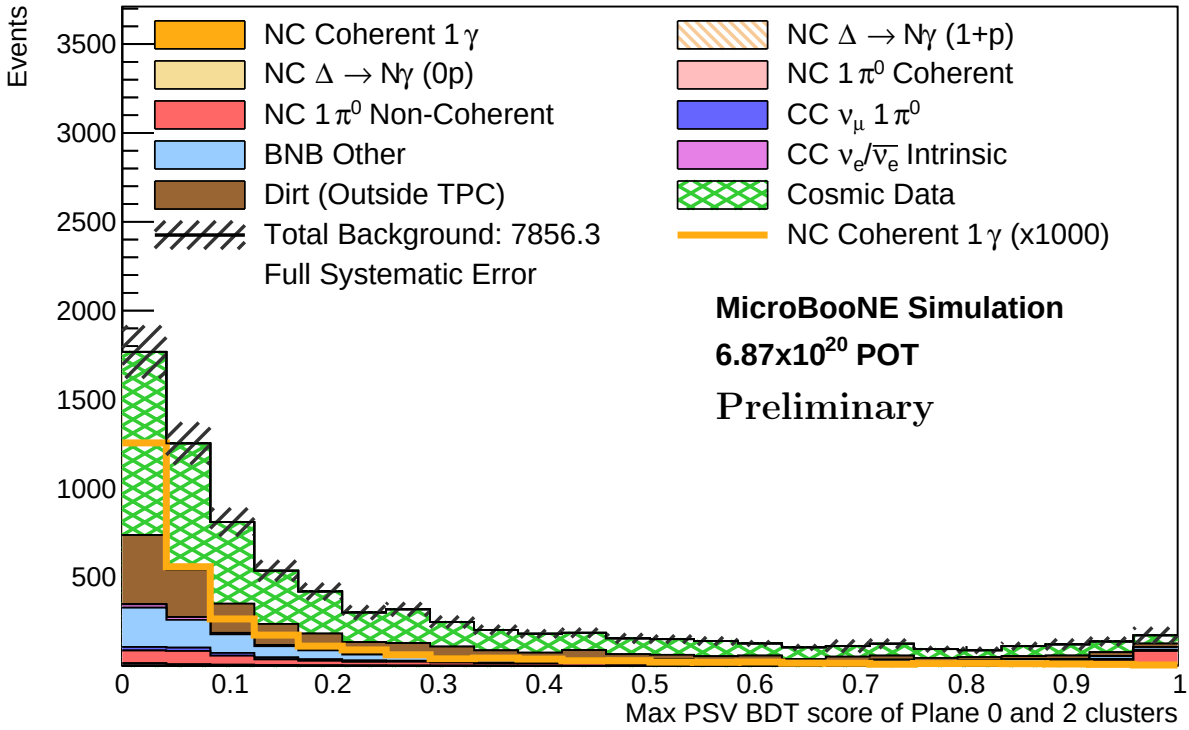

Figure 6: *The maximum PSV score among all clusters on plane 0 and plane 2 for events at preselection stage. Higher score indicates increasing confidence there is proton exiting the nucleus that is missed by Pandora. Nominal predictions for backgrounds are stacked in colored histograms, while the signal prediction is scaled by a factor of 1000 and plotted separately in the yellow hollow histogram.*

Stage	Semi-Final	Final
NC coherent 1γ (Signal)	1.3	1.1
NC $\Delta \to N\gamma$ (1+p)	0.3	0.1
NC $\Delta \to N\gamma$ (0p)	2.5	1.3
NC 1π^0 Non-Coherent	29.9	15.8
NC 1π^0 Coherent	3.8	3.1
CC ν_μ 1π^0	5.0	3.6
CC ν_e and $\overline{\nu}_e$	0.6	0.4
BNB Other	3.5	2.9
Dirt (outside TPC)	6.4	4.8
Cosmic Ray Data	2.4	0.8
Total Prediction (Unconstr.)	55.8	34.0
Total Prediction (Constr.)	45.8	29.0

Table 1: *The expected event rates in the semi-final and final selection for all event types, normalized to the Runs 1-3 data POT (6.87×10^{20}). The constrained total prediction is evaluated with the conditional constraint from the 2γ1p and 2γ0p samples.*

non-coherent 1π^0 backgrounds, with corresponding rejection efficiency of 68.8%, 47.9% and 47.4% respectively. Note that NC $\Delta \to N\gamma$ (0p) consists of NC Δ radiative decay events with exiting neutrons out of the nucleus as well as NC Δ radiative decay events with exiting protons with KE $<$ 50 MeV, the latter of which is specifically targeted by the PSV. Overall, compared to the topological selection, the final selection achieves 97.5% rejection efficiency on NC non-coherent

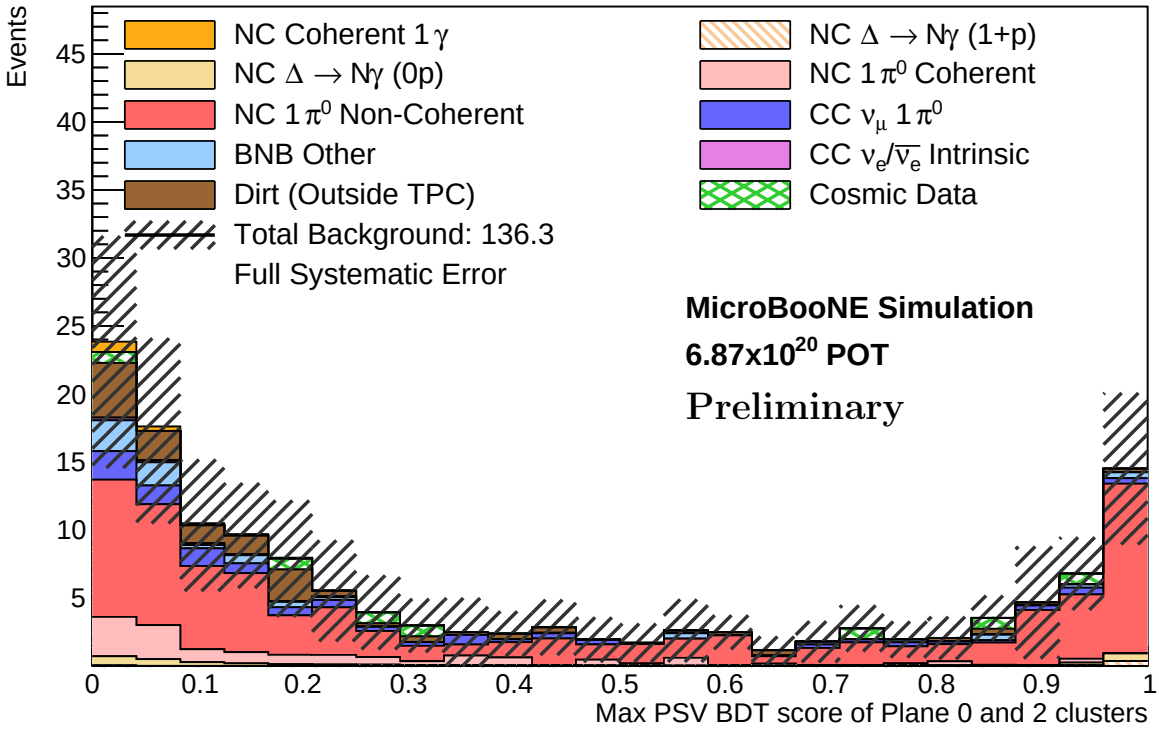

Figure 7: *The maximum PSV score among all clusters on plane 0 and plane 2 for events passing the three event-level BDTs (cosmic, CC ν_e and CC ν_μ focused BDTs). Nominal prediction for the signal is on top of the background stacked histograms shown as orange filled histogram, which can be seen on the first bin on the left.*

$1\pi^0$ and 99.99% rejection efficiency on the cosmic background while keeping the signal efficiency at 39%.

Category	preselection stage Eff [%]	Semi-Final Eff. [%]	Final Eff. [%]
NC Coherent 1 γ	98.59	45.85	39.09%
NC $\Delta \to N\gamma$ (0p)	98.30	19.18	9.99
NC $\Delta \to N\gamma$ (1+p)	97.13	7.99	2.49
NC 1 π^0 Coherent	96.91	8.38	6.83
NC 1 π^0 Non-Coherent	96.39	4.75	2.50
CC $\nu_\mu 1\pi^0$	90.21	3.07	2.24
BNB Other	82.17	0.30	0.25
CC $\nu_e/\overline{\nu}_e$ Intrinsic	94.59	0.69	0.47
Dirt (Outside TPC)	61.67	0.25	0.18
Cosmic Data	61.01	0.03	0.01

Table 2: *Selection efficiencies for signal and background categories at different stages of the analysis, calculated with respect to selections of events after topological requirement.*

4 Sideband Validation

The analysis is designed as a blind analysis, where 10% of the total data during the first run periods is open and utilized to develop the analysis and validate the agreement between data and

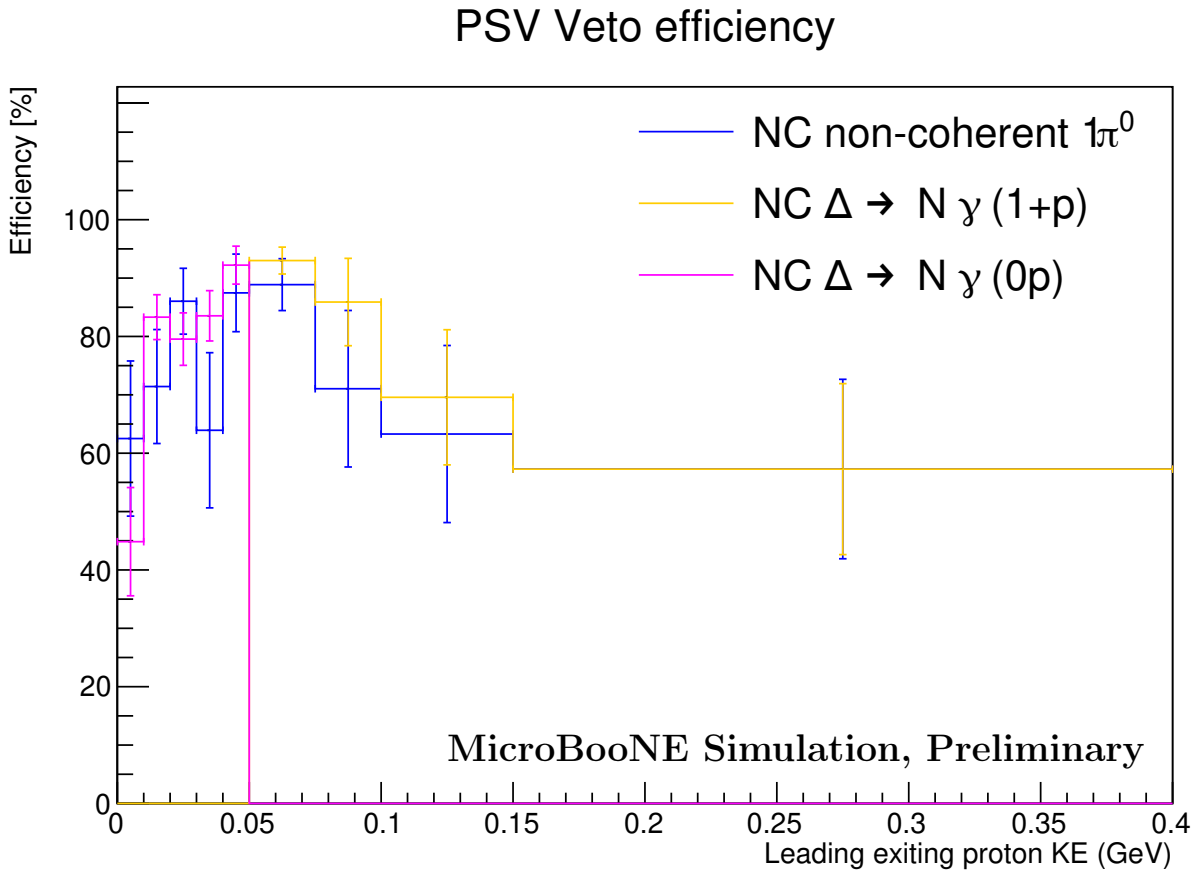

Figure 8: *The rejection efficiency of the PSV BDT as a function of the kinetic energy of the leading proton exiting the nucleus. Note that, NC $\Delta \rightarrow N\gamma$ (0p) contains events with exiting protons (with kinetic energy less than 0.05 GeV), hence the pink line representing the rejection efficiency on NC $\Delta \rightarrow N\gamma$ (0p) only extends to 0.05 GeV. The rejection efficiency on the complementary NC $\Delta \rightarrow N\gamma$ (1+p) sample instead starts from proton kinetic energy of 0.05 GeV (in yellow). The error bar represents the uncertainty arising from finite MC simulation statistics.*

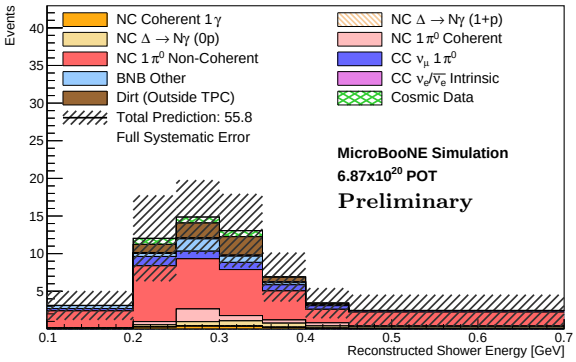

(a) Reconstructed Shower Energy

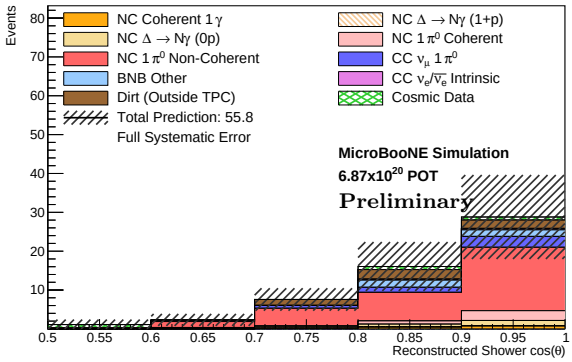

(b) Reconstructed Shower cos(θ)

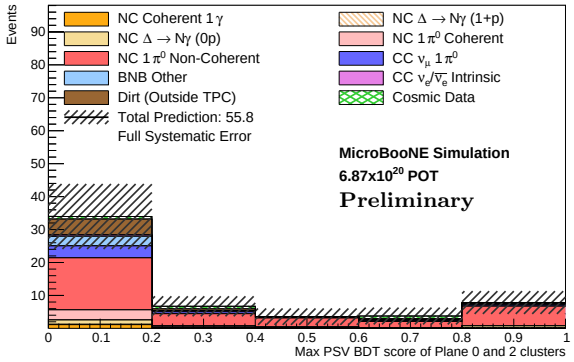

(c) Maximum PSV Score on Planes 02

Figure 9: *Distributions of semi-final selection in: (a) reconstructed shower energy; (b) reconstructed shower cos(θ); and (c) the maximum PSV score on Planes 02. The selected events have reconstructed shower with energy peak at ∼ 300 MeV in very forward directions, which is expected for the NC coherent 1γ signal. The distribution of the maximum PSV score on Planes 02 suggests the PSV cut at 0.2 could reject a significant fraction of NC non-coherent 1π⁰ background.*

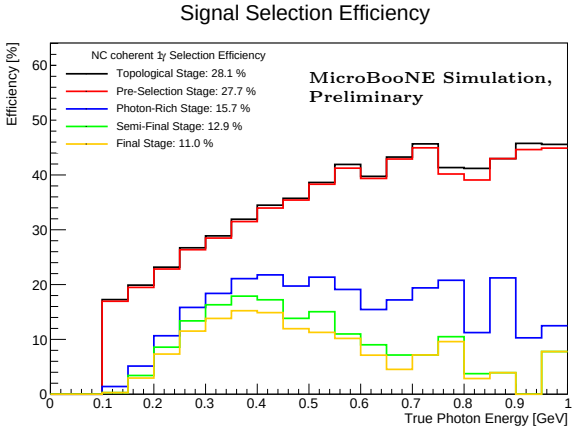

Figure 10: *Efficiencies at various stages of the selection for the NC coherent 1γ signal as a function of true photon energy The "photon-rich stage" refers to the stage where the three event-level BDTs (cosmic, CC ν_e and CC ν_μ focused BDTs) are applied. The efficiencies are calculated using the selected NC coherent 1γ within the range plotted for each variable with respect to the total prediction of NC coherent 1γ.*

MC simulation in variables of interest and input variables to all BDTs involved. The analysis selections presented and the backgrounds involved are similar to those of Ref. [4], and the NC π^0 and BNB Other backgrounds with single shower topology are validated in [4]. The performance

of the shower energy reconstruction and validation of NC π^0 modeling are demonstrated in the $2\gamma 1p$ and $2\gamma 0p$ NC π^0 measurements [10].

Here, to validate the performance of the PSV BDT, after topological and preselection stage cuts, we isolate a sideband that is proton-rich by reversing the cut on the NC π^0 BDT (<0.891) while relaxing cuts on other event-level BDTs: Cosmic BDT >0.8., CC ν_μ BDT >0.8, CC ν_e BDT >0.5. A total of 850.0 events are predicted, of which 54.0% events are predicted to have protons exiting the nucleus (regardless of proton KE). Consistency between data and MC simulation is inspected through the goodness-of-fit test that incorporates systematic uncertainties and Combined-Neyman-Pearson statistical uncertainty [11]. Figure 11 shows the distributions of the reconstructed shower energy, angle, and the maximum PSV score on Planes 02 for the sideband sample. A mild deficit in data is observed in the region of high PSV score; the subsample of events with high PSV score (above 0.8) is isolated and is found to be flat in kinematic variables. Overall, the data-MC simulation agreement for the PSV variable is good, with corresponding $p^{\text{value}} = 0.78$ when full systematic uncertainty is taken into account. Consistency in event-level and cluster-level variables including all BDT input variables is inspected, and good agreement is observed within systematic uncertainty.

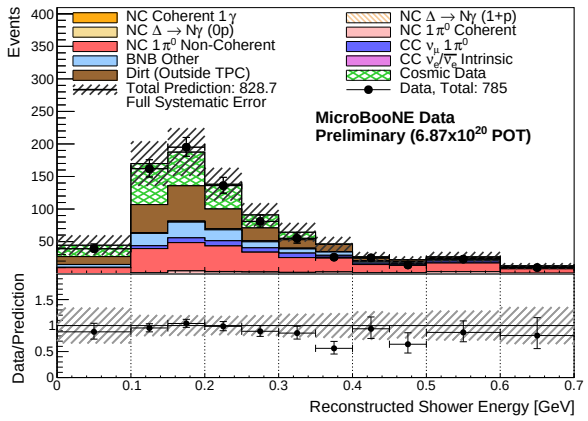

(a) Reconstructed Shower Energy

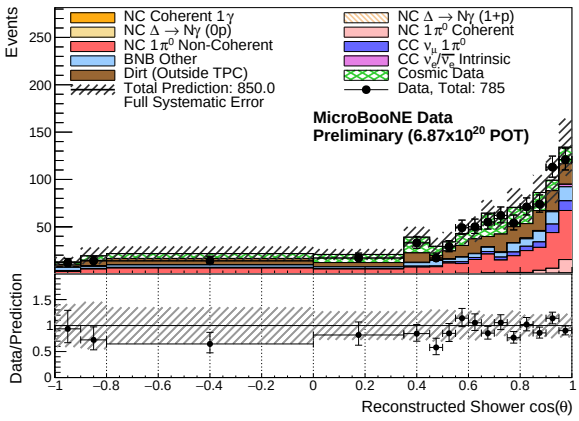

(b) Reconstructed Shower cos(θ)

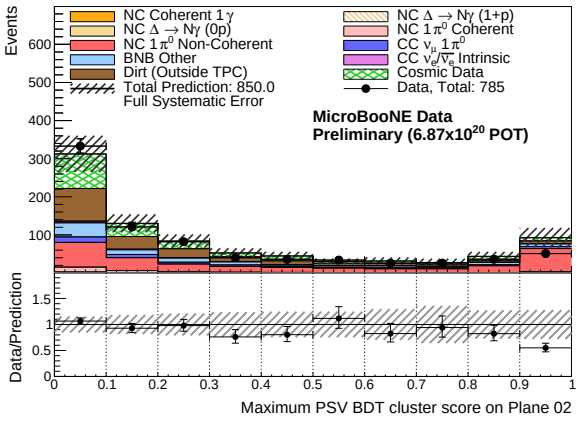

(c) Maximum PSV score on Plane 02

Figure 11: *Distributions of the sideband sample in: (a) reconstructed shower energy; (b) reconstructed shower cos(θ); and (c) the maximum PSV score on Plane 02. A mild data deficit is observed in the highest PSV score bin, but data is found to be consistent with prediction within systematic uncertainty over all three variables.*

5 Summary

In this note we have described the world's first search for the neutrino-induced NC coherent single photon process with a single shower topology and no other interaction vertex activity. Differences in the shower kinematic properties between the shower originating from coherent photons and that from other backgrounds are leveraged to yield effective background removal, leading to 99.97% and $> 95\%$ rejection efficiency on the cosmic background and NC non-coherent $1\pi^0$ relative to topological selection. Furthermore, tools utilizing low-level information are developed to identify and reject low-energy proton traces near the vertex, which further reduces the dominant NC non-coherent $1\pi^0$ background by 48%. The analysis has been fully developed and validated on both a small sample of open data, as well as dedicated sidebands sames to build confidence in our background modelling. This was especially important for the new proton veto tool developed in this analysis, which has shown great potential in rejecting low-energy protons and can be easily adapted to other coherent interaction searches.

References

[1] E. Wang, L. Alvarez-Ruso, and J. Nieves, "Photon emission in neutral-current interactions at intermediate energies," *Phys. Rev. C*, vol. 89, p. 015503, Jan 2014.

[2] E. Wang, L. Alvarez-Ruso, and J. Nieves, "Single photon events from neutral current interactions at MiniBooNE," *Phys. Lett. B*, vol. 740, pp. 16–22, 2015.

[3] A. R. *et al.*, "Design and construction of the microboone detector," *Journal of Instrumentation*, vol. 12, p. P02017, feb 2017.

[4] P. Abratenko *et al.*, "Search for neutrino-induced neutral-current Δ radiative decay in microboone and a first test of the miniboone low energy excess under a single-photon hypothesis," *Phys. Rev. Lett.*, vol. 128, p. 111801, Mar 2022.

[5] A. A. Aguilar-Arevalo *et al.*, "Updated miniboone neutrino oscillation results with increased data and new background studies," *Phys. Rev. D*, vol. 103, p. 052002, Mar 2021.

[6] L. Alvarez-Ruso *et al.*, "Recent highlights from genie v3," *The European Physical Journal Special Topics*, vol. 230, pp. 4449–4467, Dec 2021.

[7] R. Acciarri *et al.*, "The pandora multi-algorithm approach to automated pattern recognition of cosmic-ray muon and neutrino events in the microboone detector," *The European Physical Journal C*, vol. 78, p. 82, Jan 2018.

[8] P. Abratenko *et al.*, "Cosmic Ray Background Rejection with Wire-Cell LArTPC Event Reconstruction in the MicroBooNE Detector," *Phys. Rev. Applied*, vol. 15, no. 6, p. 064071, 2021.

[9] T. Chen and C. Guestrin, "Xgboost: A scalable tree boosting system," in *Proceedings of the 22nd ACM SIGKDD International Conference on Knowledge Discovery and Data Mining*, KDD '16, ACM, Aug. 2016.

[10] P. Abratenko *et al.*, "Measurement of neutral current single π^0 production on argon with the microboone detector," *Phys. Rev. D*, vol. 107, p. 012004, Jan 2023.

[11] X. Ji, W. Gu, X. Qian, H. Wei, and C. Zhang, "Combined neyman-pearson chi-square: An improved approximation to the poisson-likelihood chi-square," *Nuclear Instruments and*

Methods in Physics Research Section A: Accelerators, Spectrometers, Detectors and Associated Equipment, vol. 961, p. 163677, 02 2020.